

Light manipulation with encoded plasmonic nanostructures

Chenglong Zhao^{1,a}, Jiasen Zhang^{1,2}, and Yongmin Liu^{3,4,*}

¹ State Key Laboratory for Mesoscopic Physics, Department of Physics, Peking University, Beijing 100871, China

² Collaborative Innovation Center of Quantum Matter, Beijing 100871, China

³ Department of Mechanical and Industrial Engineering, Northeastern University, Boston MA 02115, USA

⁴ Department of Electrical and Computer Engineering, Northeastern University, Boston MA 02115, USA

Received 28 June 2014 / Accepted 20 October 2014

Abstract – Plasmonics, which allows for manipulation of light field beyond the fundamental diffraction limit, has recently attracted tremendous research efforts. The propagating surface plasmon polaritons (SPPs) confined on a metal-dielectric interface provide an ideal two-dimensional (2D) platform to develop subwavelength optical circuits for on-chip information processing and communication. The surface plasmon resonance of rationally designed metallic nanostructures, on the other hand, enables pronounced phase and polarization modulation for light beams traveling in three-dimensional (3D) free space. Flexible 2D and free-space propagating light manipulation can be achieved by encoding plasmonic nanostructures on a 2D surface, promising the design, fabrication and integration of the next-generation optical architectures with substantially reduced footprint. It is envisioned that the encoded plasmonic nanostructures can significantly expand available toolboxes for novel light manipulation. In this review, we present the fundamentals, recent developments and future perspectives in this emerging field, aiming to open up new avenues to developing revolutionary photonic devices.

Key words: Nanophotonics, Plasmonics, Surface Plasmons, Metasurface, Nanostructures.

1 Introduction

Plasmonics focuses on the novel properties and applications of surface plasmon polaritons (SPPs) that are electromagnetic modes occurring on a metal surface. This new research field has generated many breakthroughs in different disciplines, ranging from nano optics [1], energy harvesting [2, 3] and optical metamaterials [4–7] to super-resolution imaging [8–11], and ultra-sensitive biomedical detection [12–15]. Plasmonics provides a unique way to manipulate light at truly nanoscales beyond the diffraction limit. The propagating SPPs confined on a metallic-dielectric surface can be considered as two-dimensional (2D) light waves, rendering them attractive for developing next-generation ultra-small, ultra-fast integrated photonic circuits where light and electric signals can be transferred and processed simultaneously. The localized SPPs, with electromagnetic fields well confined on a metallic nanostructure, reradiate light into free space with its amplitude and phases tunable through changing the geometry of the nano-

structure. In particular, it has been shown that complete phase modulation (from 0 to 2π) is possible by rationally designed nanostructures [16, 17]. Therefore, plasmonics provides a powerful approach for controlling both the field profile and the polarization state of free-space propagating light.

It is striking that both the 2D and free-space propagating light can be well controlled by encoding 2D metallic surfaces with nanostructures of varying geometries, termed as metasurfaces by Capasso's group [16, 17]. The 2D planar configuration considerably reduces the thickness of the plasmonic devices and makes fabrication much easier compared to conventional bulk refractive elements. In addition, both the 2D and free-space light manipulation with plasmonic nanostructures benefits from the rapid development of various powerful electromagnetic (EM) simulation methods, such as finite-difference time-domain (FDTD), finite element method (FEM), boundary element method (BEM), et al. The affordable commercial EM simulation packages based on these algorithms can simulate fairly complex structures, provide important guidelines in the prototype design, and simplify the device optimization. Mature nano-fabrication techniques, such as electron beam lithography and focused ion beam milling, have been routinely applied to implement the planar nanostructures.

Thanks to the advances of the aforementioned technologies, light manipulation with novel plasmonic structures has shown a rapid development recently. Therefore, it is a good

* e-mail: y.liu@neu.edu

^a Chenglong Zhao is currently a guest researcher in the Physical Measurement Laboratory, National Institute of Standards and Technology, Gaithersburg, Maryland 20899, United States. This paper is written as individual and not based on the research in the National Institute of Standards and Technology.

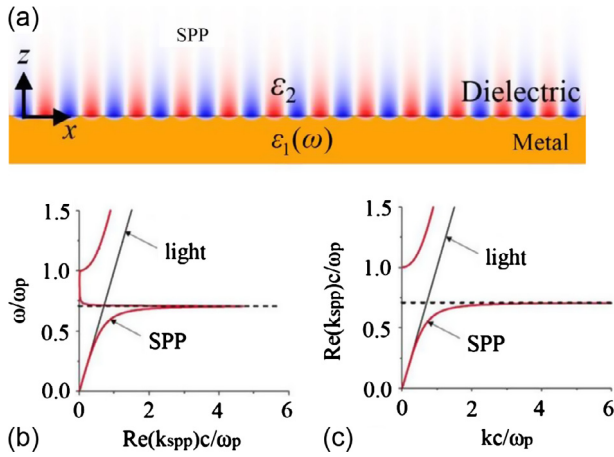


Figure 1. (a) Schematic of propagating SPPs on a metal-dielectric interface. Dispersion of SPPs propagating along a metal-air interface for (b) real frequency and complex wave vector, and (c) complex frequency and real wave vector. The flat asymptote dashed line represents the non-retarded surface plasmon solution. The straight solid line represents the dispersion curve of free-space propagating light. Reprinted from reference [18] with permission.

timing to write a review on the latest research activities in the field of light manipulation based on encoded plasmonic nanostructures. We begin with a description of the theory of plasmonics (Sect. 2), followed by a discussion about several newly developed techniques to launch unidirectional SPPs (Sect. 3), a key step for coupling free-space propagating light into 2D SPP fields. In Section 4, we review several functional plasmonic devices consisting of encoded metallic nanostructures that enable to flexibly manipulate 2D SPPs for building next generation plasmonic circuits. We also review flexible free-space light manipulations based on the encoded metallic nanostructures in Section 5. Finally, we conclude by providing perspectives for the future developments in this promising field.

2 Theory

A simple structure that can support propagating SPPs is a flat metal-dielectric interface as schematically shown in Figure 1a. The upper half space ($z > 0$) has a positive dielectric constant ϵ_2 and the lower half space ($z < 0$) is a metal that has a complex dielectric function $\epsilon_1(\omega)$. The dispersion relation of SPPs that propagate along the x direction of a 2D flat surface is [19]:

$$k_{\text{spp}} = \frac{\omega_0}{c} \sqrt{\frac{\epsilon_1 \epsilon_2}{\epsilon_1 + \epsilon_2}}, \quad (1)$$

where ω_0 is the free-space angular frequency. When dealing with a lossless metal with a real value of ϵ_1 , the square-root in equation (1) is a real number and results in a unique solution [18]. When taking the losses into account, the square-root is a complex number and it is necessary to use either a complex frequency ω_0 or complex wave vector k_{spp} [18]. Figure 1b depicts the dispersion curve of SPPs propagating along a metal-air interface with real frequency ω_0 and complex wave vector k_{spp} . The curve exhibits a back bending

around the frequency of non-retarded surface plasmon $\frac{\omega_p}{\sqrt{2}}$. Figure 1c plots the SPP dispersion curve with complex frequency ω_0 and real wave vector k_{spp} . The difference between the two curves originates from the fact that the surface plasmon interaction must be characterized by a complete response-function surface as a function of ω_0 and k_{spp} rather than by a single dispersion curve [20]. The curves shown in Figures 1b and 1c are a cross section of the response-function surface with one axis fixed [21].

Taking metal losses into account, ϵ_1 is a complex number and can be written as $\epsilon_1(\omega) = \epsilon_{1r} + i\epsilon_{1i}$. Choosing ω_0 real and $k_{\text{spp}} = \beta_r + i\beta_i$, we obtain:

$$\beta_r = k_0 \sqrt{\frac{\epsilon_{1r}\epsilon_2}{\epsilon_{1r} + \epsilon_2}}, \quad (2)$$

$$\beta_i = k_0 \left(\frac{\epsilon_{1r}\epsilon_2}{\epsilon_{1r} + \epsilon_2} \right)^{\frac{3}{2}} \frac{\epsilon_{1i}}{2\epsilon_{1r}}. \quad (3)$$

β_i determines the SPP propagating loss and we can define the SPP propagating length L_{spp} as $L_{\text{spp}} = 1/(2\beta_i)$. Therefore, SPPs travel along the metal-dielectric interface with a finite distance. At optical wavelengths, the SPP propagating length is typically in the range of 10–100 μm , which strongly depends on the materials and structures. The excellent field confinement and reasonably long travelling distance render SPPs a good candidate for designing plasmonic integrated circuits where electric and optical signals can be transferred simultaneously [22].

A nanohole on a 2D metal surface can be treated as a SPP point source. The SPP fields generated from such a SPP point source has a larger angular distribution, showing a pattern similar to that from an in-plane dipole and known analytically [23, 25]. Figure 2a shows the calculated SPP fields generated from a nanohole with FDTD. Assuming a nanohole located at origin is illuminated by a x polarized light, the resulting SPP fields can be approximately expressed as follows [23]:

$$E_{\text{spp}} = A \left(\hat{z} - \frac{ik_{zi}}{\beta_r} \hat{\rho} \right) H_1^{(1)}(\beta_r \rho) \cos(\varphi) e^{-k_{zi}z} e^{-i\omega t}, \quad (4)$$

where $(\hat{\rho}, \hat{\varphi}, \hat{z})$ are the vector units under cylindrical coordinates (ρ, φ, z) . A is a constant, $H_1^{(1)}(k_{\text{spp}}\rho)$ is the $m = 1$ Hankel function. β_r is the real part of the SPP wave vector defined in equation (2). k_{zi} is the z -component of the wave vector defined by $k_{zi}^2 = k_{\text{spp}}^2 - k_0^2\epsilon_i$. Figure 2b shows the calculated SPP fields using FDTD (symbols) and equation (4) (solid curves). The SPP fields calculated with the analytical equation (4) agree well with that of the FDTD simulation as long as the field position is larger than 100 nm. Zhang's group [24, 26–30] has shown that the SPP fields launched from an arbitrary slit on a 2D metal surface, such as a SPP Fresnel zone plate [24] illustrated in Figure 2c, can be calculated by applying the Huygens-Fresnel principle. Every point of the slit can be considered as a secondary SPP point source with fields described by equation (4). The resulting fields can be obtained by summing up the fields from all the SPP point sources and taking into account their phase and amplitude. Figure 2d presents the experimental leakage radiation microscopy (LRM) image of SPPs launched from the Fresnel zone plate. LRM is a powerful and convenient technique for

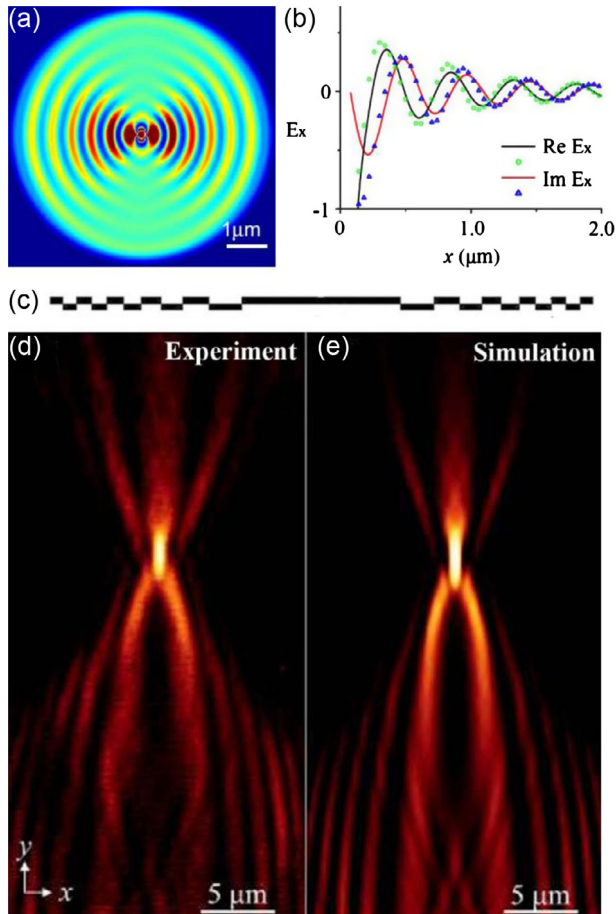


Figure 2. (a) Calculated SPP fields from a nanohole with FDTD. (b) Comparison of SPP fields calculated with FDTD (symbols) and analytical equation (solid curve). Reprinted from reference [23] with permission. (c) Structure of a SPP Fresnel zone plate (FZP). (d) Leakage radiation image of SPPs launched from the FZP. (e) Calculated SPP fields of the FZP by applying Huygens-Fresnel principle. Reprinted from reference [24] with permission.

detecting SPP field. The SPPs on the top interface of a thin metal film can radiatively leak through the film and the substrate, and finally be collected by an oil-immense lens with high numerical aperture. It allows fast mapping the SPP near-field in the way of far-field detection, compared to other time-consuming scanning techniques, such as near-field scanning optical microscope (NSOM). We refer the readers to some early work for more details about this technique [31–35]. Figure 2e shows the corresponding SPP fields calculated by applying Huygens-Fresnel principle. The simulation almost perfectly matches with the experimental results and well reproduced the detailed SPP pattern. The advantage of using this method arises from the fact that it can significantly reduce the simulation time and save computation resources compared to that calculated with other numerical methods such as FDTD or FEM. The typical length of the structures as shown in Figure 2c is tens of micrometers so that FDTD or FEM has difficulties in handling such large simulation domains on a personal computer. In contrast, it can be easily calculated with the Huygens-Fresnel method.

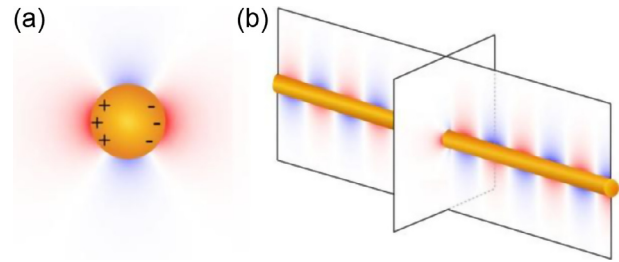


Figure 3. (a) Schematic of localized surface plasmons supported by a metallic nanoparticle. (b) Schematic of hybrid plasmonic mode of propagating and localized surface plasmons supported by a metallic nanowire.

Another type of surface plasmons, so-called localized surface plasmons, are supported by metallic nanostructures as schematically illustrated in Figure 3a. The electron oscillation induced by the incident light is confined on the surface of the nanoparticles, which results in strong plasmonic resonance at particular wavelengths, depending on the material and geometry of the nanostructures. The phase and amplitude of the reemitted light can be readily tuned by changing the shape of the structure. This tunability enables manipulation of free-space propagating light through rationally encoding nanostructures on a 2D surface, which will be reviewed in Section 5. Another type of surface plasmons supported by one-dimensional metallic structures, i.e. nanowires, is a hybridization of localized and propagating SPPs as shown in Figure 3b. The lateral dimension of the nanowire is small enough to support localized surface plasmons; while the length of the nanowire is large enough to support propagating surface plasmons. Such surface plasmons are introduced here for completeness but will not be discussed in this review. We refer readers to the recent review papers [36, 37] for more insights in the application of this type of surface plasmons.

3 SPP unidirectional excitation

Having discussed the fundamentals of SPPs, now we will review the different aspects of light manipulation based on metallic nanostructures. For integrated plasmonic circuits, one indispensable plasmonic element is an efficient SPP source. There has been intensive effort in the plasmonic community to develop laser equivalent SPP light source, so-called SPP laser or spaser [38–45]. However, it is still under development and far from mature. A common and convenient way of generating SPPs is converting free-space propagating light into 2D SPPs. SPPs cannot be directly launched on a smooth metal-dielectric interface without playing some tricks, such as using nonlinear optical method [46], because of the wave vector mismatch between free-space light and SPPs as indicated in the dispersion diagram in Figures 1b and 1c. Therefore, gratings and nanostructures are commonly used to launch SPPs on a metal-dielectric surface through diffracting the free-space propagating light and providing an additional in-plane wave vector to compensate the wave vector mismatch between the free-space light and SPPs. There are alternative methods to launch SPPs, such as prism coupling or tip scattering [19].

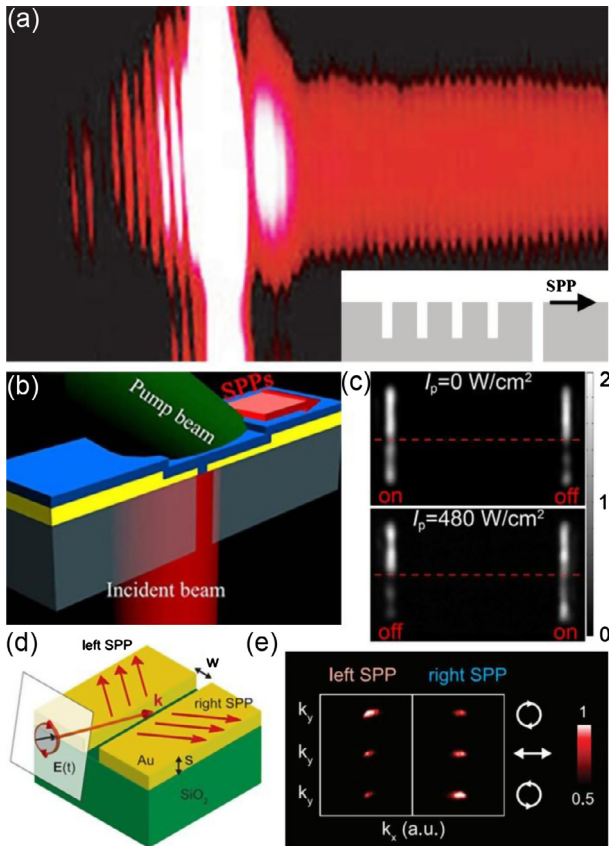


Figure 4. SPP unidirectional excitation. (a) SPPs launched from a Bragg reflection grating. (b) Schematic of a T-shaped single slit for SPP unidirectional excitation. (c) SPP intensities launched from a T-shaped single slit that are finally scattered from a decoupling grating for two different pump intensities. (d) Schematic of a single slit illuminated by circular polarized light to excite unidirectional SPPs. (e) The experimental results of controllable SPP excitation in (d) under the illumination with different polarization states. Reprinted from references [47–49] with permission.

However, the advantages of using gratings and nanostructures lies in the device minimization and integration, since these structures can be readily fabricated on a metal film with standard nanofabrication technology. The gratings and nanostructures serve as indirect SPP sources. SPPs are launched from these structures with direct illumination and the phase and amplitude of SPPs can be precisely controlled by arranging the geometry and position of the SPP sources, making diverse SPP manipulation on metal surface possible.

Once SPPs are excited, they typically propagate from both sides of a symmetric nanostructure or grating under the condition of normal incidence. This bidirectional excitation limits some applications where directional SPP beams are required. Therefore, several unique SPP launching structures have been designed to achieve unidirectional SPP excitation. The bidirectional SPP excitation from a conventional slit originates from the symmetry of either the structure itself or the illumination. As a result, unidirectional SPP excitation can be realized by breaking the geometry or illumination symmetry. The simplest geometry that can be used to launch SPPs is a slit milled

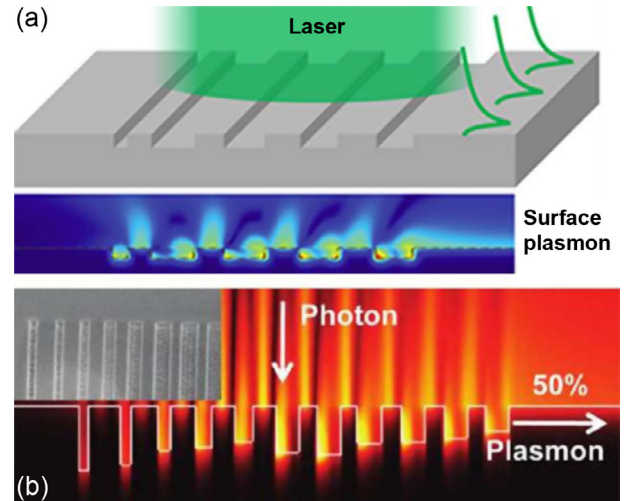


Figure 5. SPP unidirectional excitation with aperiodic grating coupler (a), and grooves with varying width and depth (b). Reprinted from references [55, 56] with permission.

through a metal film. The slit functions as a SPP line source and SPPs are launched symmetrically from both sides of the slit with normal illumination. A Bragg reflection grating fabricated next to the slit as illustrated in the inset of Figure 4a can be used to achieve unidirectional SPP excitations. Figure 4a shows the SPP field recorded with photon scanning tunneling micrographs [47, 50]. The SPPs launched from the left side of the slit are reflected back to the right side, resulting in unidirectional SPP excitation. However, the SPPs reflected from the Bragg grating cause additional scattering losses. Gong's group experimentally demonstrated a submicron bidirectional all-optical plasmonic switch with an asymmetric T-shape single slit [48]. The asymmetric T-shaped single slit was coated with a nonlinear polymer film as shown in Figure 4b. Unidirectional SPP excitation from either side of the slit can be switched by varying the real part of the polymer permittivity with a pump laser beam as shown in Figure 4c. Gong's group also reported unidirectional SPP excitation from two grooves with different depth [51]. The aforementioned structures are normally illuminated with linear polarized light. The unidirectional SPP excitation can also be realized by breaking the illumination symmetry. For instance, illuminating a spatially symmetric slit with circularly polarized light, as shown in Figure 4d, can excite SPPs predominantly propagating along one specific direction [49]. The direction of the SPP propagation is switchable with the helicity of the circular polarization as shown in Figure 4e. Unidirectional SPP excitation can also be achieved with oblique illuminations [52, 53]. Although transverse electric fields are commonly implemented to excite SPPs from a slit, Lee's group demonstrated that the transverse magnetic field component perpendicular to the direction of slit is able to efficiently excite SPPs [54].

A single nanoslit is not an effective SPP coupler. Therefore, gratings are commonly used to increase the launched SPP intensities. Asymmetric grating structures are needed in order to realize unidirectional SPP excitation. Huang et al. designed an aperiodic grating coupler composed of five

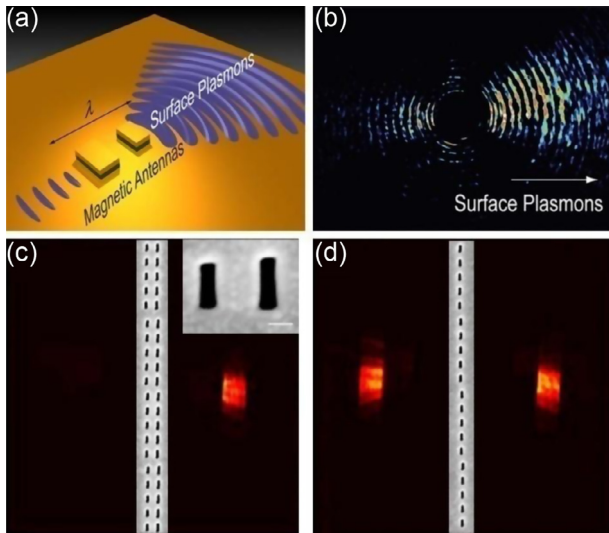


Figure 6. (a) Schematic of a magnetic antenna for unidirectional SPP excitation. (b) Leakage radiation microscopy shows the propagation of SPPs excited by the magnetic antenna. (c) Unidirectional SPP excitation with asymmetric optical slot nanoantennas. Inset shows the scanning electron microscope (SEM) image of the slot nanoantenna. (d) SPP launched from both sides of a symmetric slot nanoantenna for comparison. Inset shows the SEM image. Reprinted and modified from references [59, 60] with permission.

subwavelength grooves fabricated on silver film as shown in Figure 5a. The distances between adjacent grooves with the same depth were optimized with a transfer matrix model. The aperiodic grating enables unidirectional SPP excitation with a right-to-left contrast ratio of 55 [55]. Baron et al. reported unidirectional SPP launching with efficiency greater than 52% under normal illumination [56]. The grating consists of 11 grooves with varying width and depth as shown in Figure 5b. It enables efficient SPP excitation, and the propagating SPP can be efficiently converted back to free-space propagating light as well due to the reciprocity theorem. Slanted and ridge grating were also employed for unidirectional SPP excitation [57, 58].

The unidirectional SPP couplers made of slit or grating are not preferable for further minimization of plasmonic devices partly due to its relative large dimension along at least one direction. Considerable effort has been devoted to scale down plasmonic components into the nanometer regime. Optical antennas, properly designed resonant nanostructures, have emerged as a new scheme to manipulate the transmission and reception of optical fields at the nanoscale [61–63]. Inspired by the exceptional directionality control over radiative waves based on optical antennas, Liu et al. proposed a magnetic antenna that enables directional SPP excitations in the near field with efficiency as high as 135% when normalized to the energy illuminated on the physical area of the antennas [59]. The designed antenna consists of two nanomagnetic resonators with detuned resonant wavelengths as shown in Figure 6a. At the resonance frequency, the nanomagnetic resonator strongly interacts with light, and part of the reradiated energy will be converted into SPP modes. The excited SPPs generated by the two resonators constructively or destructively

interfere, depending on the relative phase and the separation between the two nano resonators. As a result, the propagation of SPPs can be unidirectional. Figure 6b presents the leakage radiation microscopy results for a nanoantenna that predominantly launches SPP on the right side of the antenna. In another work, Zhang’s group demonstrated unidirectional SPP excitation with an asymmetric optical slot nanoantenna [60]. The structure comprises two optical slot nanoantennas with different lengths as shown in the inset of Figure 6c. Broadband unidirectional excitation of SPPs with extinction ratio up to 44 has been achieved by properly tuning the length and distance between the two slot nanoantennas. Figure 6c shows that SPPs are mainly excited at the right side of the optical antenna. For comparison, Figure 6d shows that SPPs are launched at both sides of the antenna with a single optical slot. Recently, Zhang’s group also demonstrated broadband directional SPP excitation via L-shaped optical slot nanoantennas based on phase retardation and spectra overlapping of the plasmonic modes [64].

The unidirectional SPP couplers discussed above are sensitive to the polarization of the incident light. The coupling efficiency is maximum (minimum) if incident polarization is perpendicular (parallel) to the slit or grating. Such polarization sensitivity results in a decrease in the SPP signal and loss of polarization information of the incident light. Lin et al. [65] solved this problem by carefully designing the orientation of paired nanoslits with the launched SPPs sensitive to the handedness of the incident light as schematically shown in Figure 7a. Multiple columns of the nanoslit pairs are used to increase the SPP intensities. Figures 7b and 7c present the near-field scanning optical microscopy image of SPPs launched with right and left circular polarized light, respectively. One can clearly see that unidirectional SPP excitation and the direction of SPP excitation are well controlled by changing the helicity of the incident light. Similar results have been achieved in another different design by Huang et al. [66]. In their work, the metasurface consists of an array of elongated apertures with a constant gradient of orientation respect to the x axis as schematically shown in Figure 7d. The metasurface is designed so that the two anomalous first-order diffracted beams are not symmetric about the surface normal, and they are used to match the SPP wave vector. Figures 7e and 7f show SPPs are launched at the right or left side of the metasurface with incident helicity $\sigma = 1$ and -1 , respectively.

4 2D SPP in-plane manipulation

With the aforementioned SPP launching techniques, the next crucial step is to design functional SPP elements as building blocks to control the SPPs for next-generation on-chip plasmonic circuits. A straightforward approach to achieve this goal is fabricating functional elements directly on the SPP propagating path to modulate the SPP wavefront [67, 68], in a similar way to conventional free-space propagating light manipulation with optical elements. However, the main obstacle here is the increased scattering losses due to the abrupt discontinuity at the interface of the SPP elements. SPPs are tightly confined on the surface of the metal film, and therefore are

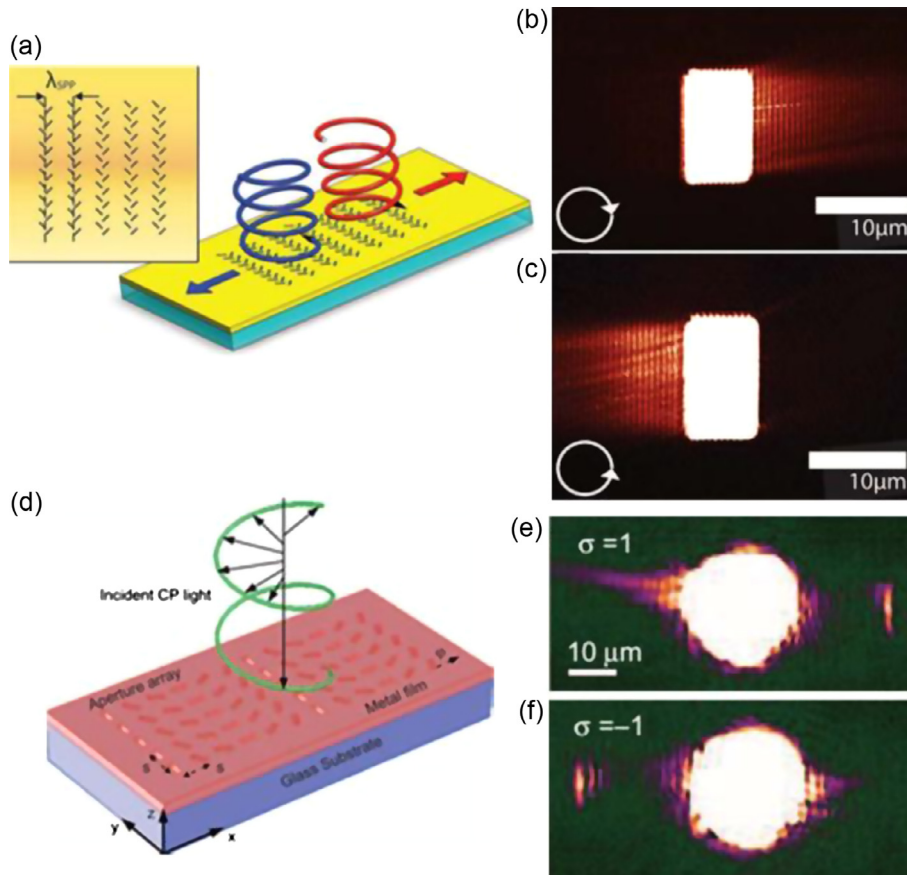


Figure 7. (a) Schematic of a metasurface enables unidirectional SPP excitation. Near-field scanning optical microscopy image shows left circular polarized light CPL is coupled to SPPs propagating to the right (b), while right circular polarized light is coupled to the SPPs propagating to the left (c). Reprinted from ref. [65] with permission. (d) Schematic of a unidirectional SPPs coupler. (e) Experimental result shows SPPs are only excited to the right direction for an incident beam with right circular polarization. (f) Experimental result shows SPPs are only excited to the left direction for an incident beam with left circular polarization. Reprinted from reference [66] with permission.

especially sensitive to the imperfection of the fabricated elements. Zentgraf et al. have solved this problem in their demonstration of plasmonic Luneburg and Eaton lenses with gradually changed indexes fabricated by grey-scale electron-beam lithography [69].

Both lenses require a gradual change of the mode index, which is realized through tailoring the thickness of a dielectric (PMMA) cladding layer on top of a gold surface. Figures 8a and 8c show the SEM image of the plasmonic Luneburg lens and Eaton lens, respectively. Figures 8b and 8d are the corresponding fluorescence imaging of SPP propagation. Fluorescence imaging of SPP propagation clearly demonstrates the function of the plasmonic Luneburg lens and Eaton lens, which focus plane-wave-like SPPs to the perimeter of the lens and bend SPPs, respectively. In addition, both lenses exhibit a reasonably broad operation wavelength range.

Another way of solving the problem of SPP scattering is modulating the SPP wavefront right at the launching position. The relative size and position of a SPP source, such as a nano-hole, determines the amplitude and phase of the launched SPPs. Therefore, it is possible to fully control the SPP

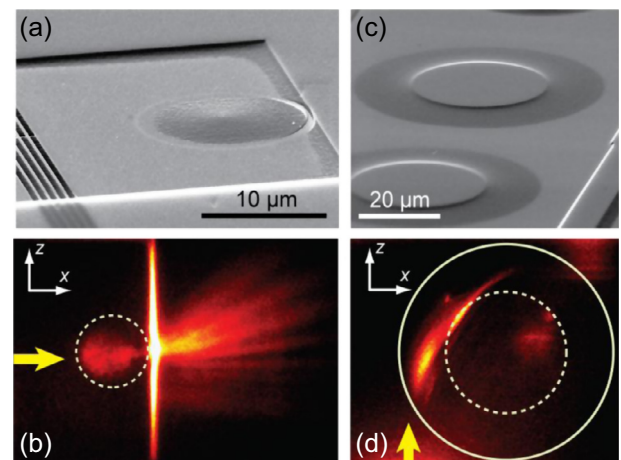


Figure 8. Scanning electron microscope image of (a) plasmonic Luneburg lens and (b) plasmonic Eaton lens. The corresponding fluorescence imaging results are shown in (c) and (d), respectively. The yellow arrow indicates the position of incident SPPs. Reprinted and modified from reference [69] with permission.

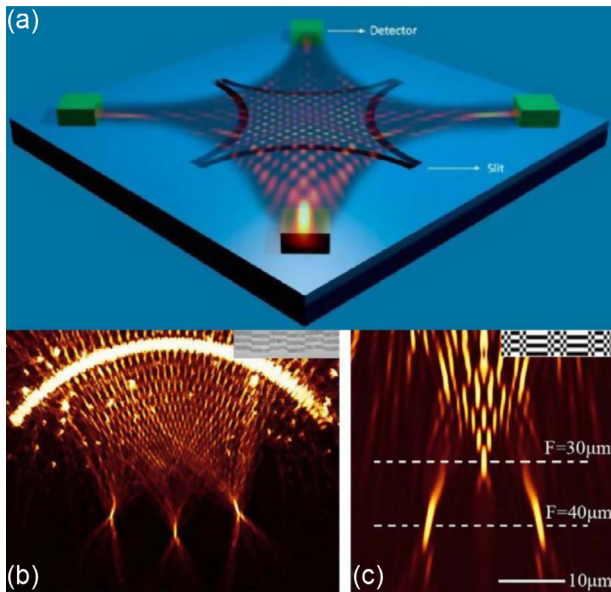


Figure 9. (a) Plasmonic splitter based on pin cushion structures. Reprinted from reference [70] with permission. (b) Leakage radiation image of SPPs from a plasmonic splitter based on concentric nanostructures. Inset shows the SEM image. Reprinted from reference [27] with permission. (c) Simulation of SPP fields from a binary plasmonic splitter. Inset shows the schematic of the binary structure. Reprinted from reference [28] with permission.

wavefront at the launching position by encoding the shape and position of the SPP sources. The scattering losses of SPPs are greatly reduced since there are no scattering structures along the propagation path. Based on this concept, several functional plasmonic devices have been demonstrated recently.

A fundamental function of a plasmonic device is focusing in-plane SPPs into a tight focal spot. This has been successfully realized by using various curved nanoslits that were fabricated on metal film [71–76]. The curved nanoslit enables focusing SPPs well into one focal spot. However, the ability of multiple focusing of SPPs is critical to achieve multi-channel SPP couplings. Therefore, a plasmonic splitter is ideal for this purpose. Lerman and Levy have developed a plasmonic splitter based on pin cushion structure as shown in Figure 9a. The pin cushion structure consists of four, quarter-circle-shaped, subwavelength slits fabricated on silver film with their centers facing to each other [70]. The direction of the generated SPPs depends on the polarization of the incident light because of the orientation of the slits. The plasmonic splitter enables SPP excitation, SPP splitting and SPP focusing simultaneously from the same structure. Zhao et al. demonstrated a plasmonic splitter based on finely designed concentric grooves that are located on a concave structure [27]. The SEM image of the structure is shown in the inset of Figure 9b. The projection of the concentric grooves forms a grating and enables launching and diffracting SPPs into different diffraction orders with equal intensities. The concaved structures guarantee that the diffracted SPPs can be focused into different SPP focal spots. Figure 9b is the leakage radiation image of SPPs that are focused into three focal spots with equal intensities. The num-

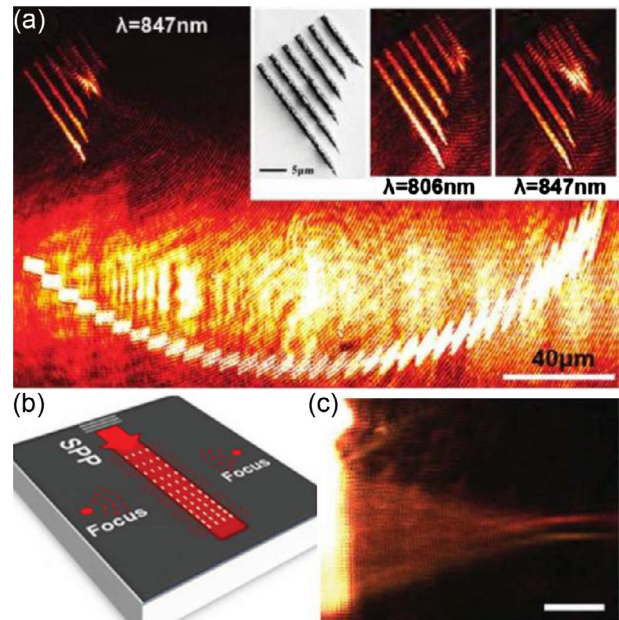


Figure 10. (a) Leakage radiation image of SPPs from a plasmonic demultiplexer based on concentric grooves. Insets show the enlarged area of the SPP waveguides. Reprinted from reference [29] with permission. (b) Schematic of a plasmonic demultiplexer based on diffracting slits. (c) Leakage radiation image shows SPPs are routed to different positions with incident light of different wavelengths. Reprinted from reference [81] with permission.

ber of SPP focal spots and their relative positions can be changed by increasing the grating pitches. Another method, so called binary plasmonics [28], was developed to produce almost arbitrary 2D SPP patterns. The design process is a back projection problem that requires calculation of the structures based on the desired SPP fields. The central principle is to pixelate the SPP launching structure and optimize the combination of these pixelated structures so that the final desired SPP patterns can be generated from the structures. The inset of Figure 9c shows a binary plasmonic structure calculated with a simulated annealing algorithm that enables focusing SPPs at different focal planes. Figure 9c depicts the calculated SPP fields that are focused into three focal spots located at different focal planes. In principle, arbitrary SPP patterns can be generated with this method. Plasmonic splitters based on Talbot effects have been demonstrated [30, 77–79]. Recently, multifunctional and multi-output plasmonic meta-elements were demonstrated based on encoded nonperiodic plasmonic arrays [80].

A plasmonic demultiplexer, a vital device for future plasmonics based optical communications, has also been realized. One plasmonic demultiplexer, which consists of concentric grooves with periodic projections on a line, allows for sorting light with different wavelengths into different plasmonic guiding channels [29]. The concentric grooves guarantee that all the launched SPPs from these grooves are well focused and the periodic projections of these grooves enable effective dispersion of the SPPs with respect to their wavelengths. Figure 10a shows the leakage radiation images of SPPs for this

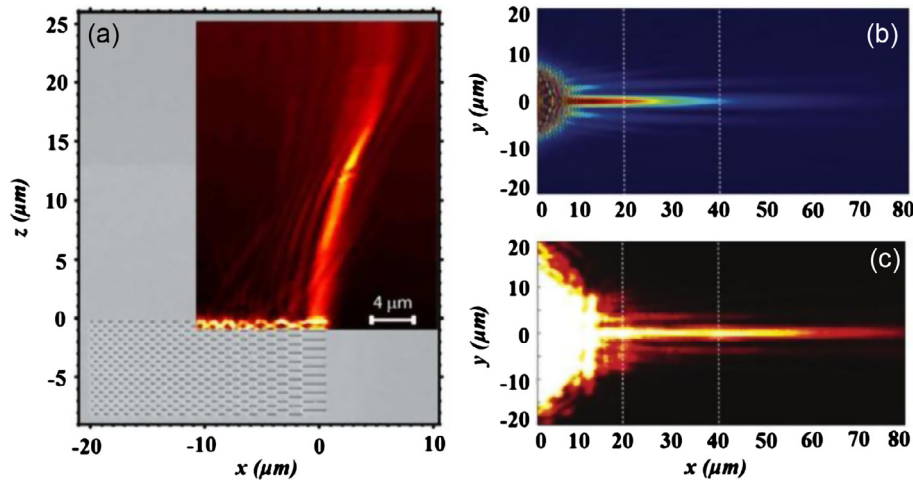


Figure 11. (a) Near-field imaging of Airy SPP beam superimposed with the WEM image of the grating pattern. Reprinted from reference [85] with permission. (b) The calculated near-field intensity distributions of the non-diffraction SPP beam. (c) Experimental near-field intensity distribution measured with near-field scanning optical microscope. Reprinted from reference [86] with permission.

plasmonic demultiplexer. Five plasmonic waveguides are integrated within the demultiplexer and placed around the SPP focal spots. It appears that SPPs with different wavelengths are routed into different SPP waveguides, a typical functionality of a demultiplexer. Li et al. [81] used a nonlinear phase modulation method to realize the function of a plasmonic demultiplexer. SPPs launched from a grating pass through a row of nanoarray with local lattice parameter gradually changed in the wave propagation direction as schematically illustrated in Figure 10b. The nanoarray is arranged with almost linear distance increment along the SPP propagation so that a square phase evolution is achieved after SPP passing through the nanoarray. Therefore, the nanoarray is capable of focusing SPPs with a broad bandwidth (100 nm) into different location. Figure 10c shows the leakage radiation image of SPP demultiplexing with two free-space incident wavelengths of $\lambda_1 = 633$ nm and $\lambda_2 = 594$ nm. The resolution of the plasmonic demultiplexer is 12 nm. Plasmonic demultiplexers with other nanostructures, such as nonperiodic nanoslits [82], subwavelength metal grooves [83] and an array of closely packed antennas [84], have also been demonstrated.

Recently, there have been great efforts to develop methods to achieve diffraction-free SPP beams that have a transverse intensity distribution independent of the propagation distance. As a result, we can suppress the spreading of SPPs as they propagate and improve the coupling between on-chip plasmonic components. In 2011, three groups [85, 87, 88] independently demonstrated nondiffracting SPP beams, so-called plasmonic airy beams that was originally proposed by Salandrino and Christodoulides [89]. The plasmonic airy beams exhibits significant beam bending over their propagation path, as one can see from the near-field image of the plasmonic airy beam in Figure 11a [85]. An interesting property of a plasmonic airy beam is self-healing, namely, the beam recovers its shape after passing through a defect. We refer readers to a latest review paper for more insights on the plasmonic airy beams [90]. A nonperfectly matched Bragg diffraction method was also developed for diffraction-free SPP beams [91].

Capasso's group demonstrated a localized long-range non-diffracting SPP waves based on two intersecting metallic launching gratings [86]. Figures 11b and 11c show the calculated and experimental near-field intensity distributions of the localized long-range non-diffracting SPP beams, respectively. The SPP can propagate as long as 80 μm without significant diffraction. Alternatively, SPPs propagating on a metal film can also be converted to arbitrary shaped free-space light. For example, Dolev et al. have demonstrated controlling the amplitude and phase of the free-space beam that converted from SPPs by employing a grating designed by holographic techniques [92]. In this way, the inputs and outputs of the plasmonic circuit can compatibly interact with arbitrary-shaped free-space propagating light.

The aforementioned work represents a major step towards 2D SPP manipulations. The functionality of the plasmonic devices is typically fixed once the plasmonic structures are fabricated on the metal film. Considering practical applications, it is beneficial to develop tunable and multi-functional plasmonic devices. Extensive effort has been devoted in order to dynamically control the resonance or propagation of SPPs by various functional media and response mechanisms [94, 95]. Recently, a reconfigurable plasmofluidic lens has been successfully demonstrated [93]. Laser-induced surface bubbles on a metallic-liquid surface as schematically shown in Figure 12a are used to manipulate the propagation of SPPs. SPP divergence, collimation, and focusing are all achieved by such a reconfigurable plasmofluidic lens via precisely controlling the size, location and shape of the surface bubbles, as well as the phase front of the incident SPPs. Figure 12b shows SPP focusing with an arc grating without the surface bubble. Figures 12c–12e show the dynamic SPP manipulation with a tunable surface bubble. The initially focused SPPs are gradually collimated as the surface bubble shrinks. The naturally smooth contact of surface bubbles with the gold film could help to reduce the scattering loss in conventional plasmonic elements with abrupt discontinuities. The shape of surface bubbles can be readily modified, which provides additional degrees of freedom

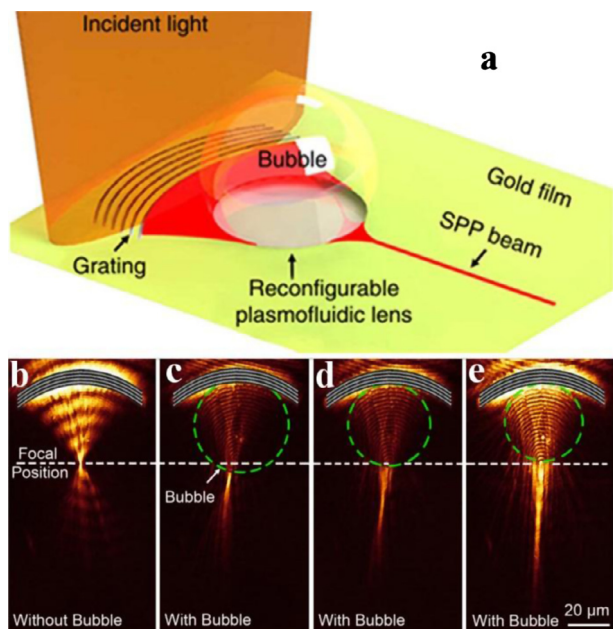


Figure 12. (a) Schematic of a reconfigurable plasmofluidic lens. (b) Leakage radiation images of SPPs focused with an arc grating without a surface bubble. (c–e) Leakage radiation images for SPPs propagating through three surface bubbles with decreasing diameters. Reprinted from reference [93] with permission.

to enrich the functionality of the plasmofluidic lens. Another way to achieve dynamic SPP manipulation is by dynamically changing the incident light with a spatial light modulator, which enables tunable plasmonic manipulation without any mechanical movement [26, 88, 96].

5 Free-space light manipulation

The interaction between incident light and plasmonic nanostructures generates localized surface plasmons, which in turn radiates light into free space. The localized surface plasmon resonance strongly depends on the shape of the metallic nanostructures, which allows both amplitudes and phase modulation (from 0 to 2π) of the re-radiated light by properly designing the nanostructures [17, 97]. Unlike conventional bulk optical elements, the plasmonic nanostructures encoded on an ultrathin, planar surface, so-called metasurface, provide a revolutionary way of steering free-space light. Conventional diffractive optical elements (DOE) that have depth controlled phase profile could also achieve full phase modulation (from 0 to 2π) with multiple phase steps. However, it typically requires several lithography steps, significantly increasing the fabrication challenge as well as cost. In contrast, metasurfaces can provide continuous phase control with a single lithography step, rendering the devices very cost effective. The planar geometry of metasurfaces is also suitable for subsequent device integration. Moreover, the polarization of the free-space propagating light can be easily tuned by changing the orientation or shape of the encoded metallic nanostructures. In comparison, it is not so straightforward for DOE, and the selective polarization is mainly achieved by introducing birefringent materials or

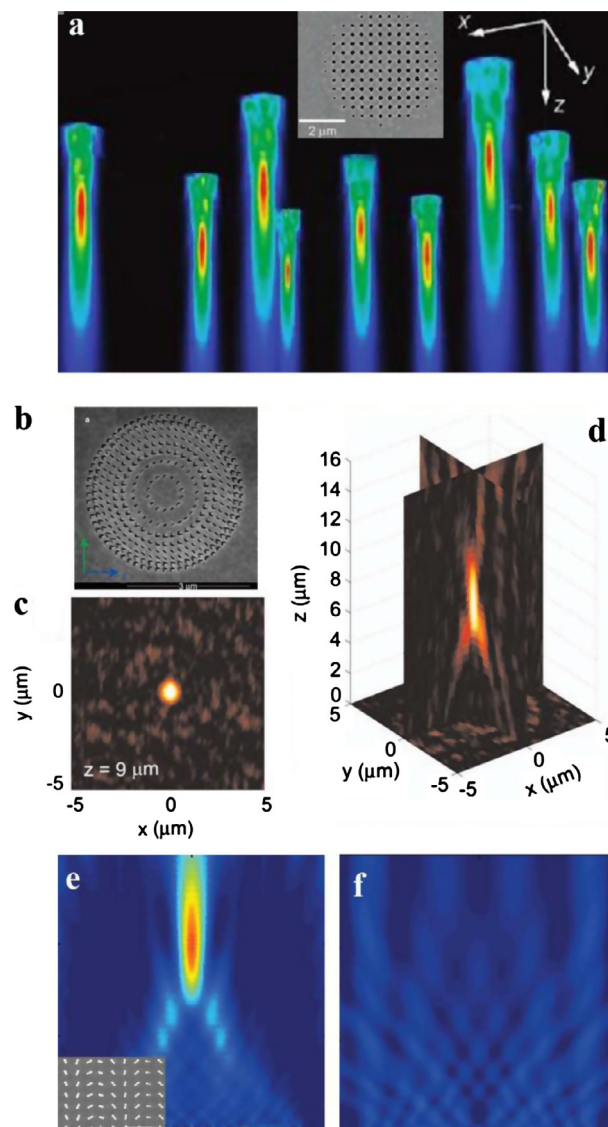


Figure 13. (a) Broadband (white) light focusing by large-area plasmonic microlens arrays. Inset shows the SEM image of a plasmonic microlens. Reprinted from reference [98] with permission. (b) SEM image of a planar plasmonic metalens. (c) The intensity profiles of the cross-polarized scattered light from the metalens at the transverse plane. (d) The intensity maps depicted on two orthogonal cross-section planes. Reprinted from reference [99] with permission. (e) Calculated intensity of a dual-polarity plasmonic lens indicates that the lens functions as a positive lens for right circularly polarized light. (f) The same lens changes its polarity and turns into a negative lens. Reprinted from reference [100] with permission.

fabricating sub-wavelength structures on an isotropic substrate to create artificial birefringence.

A simple yet indispensable function of free-space light manipulation is focusing. Conventional glass lenses achieve free-space light focusing through changing the curvature of bulk lenses. Although diffractive optical lenses have been developed to bring new functionality, their practical uses are still limited by the lack of deep phase modulation and

polarization control. Plasmonic lenses, in contrast, utilize the localized plasmonic resonance of metallic nanostructures, rendering compact, flat lenses possible. Soon after the experimental demonstration of far-field lensing using a 1D plasmonic slit array [101], similar focusing effect has been realized by 2D arrays of apertures [98, 102]. One of such designs is based on circular nanoholes as shown in the inset of Figure 13a [98]. Free-space light focusing relies on surface plasmon-mediated optical transmission. An interesting property of this microlens is that the focal spot only depends on the total size of the nanohole patch, while it is insensitive to the shape of the nanoholes. This property provides a great tolerance for fabrication. The plasmonic microlenses can focus not only single-wavelength light, but also white light with minimal chromatic aberration. In another work, Lin et al. use a 2D cross-shaped aperture array [102]. The desired spatial phase modulation for the transmitted field was achieved by changing the localized surface plasmon resonance of the cross-shaped aperture. However, the phase of these early versions of plasmonic lenses was acquired accumulatively from SPP propagating through plasmonic nanoholes and the attainable phase modulation depth is well below 2π . The recently developed metasurfaces, which comprise arrays of subwavelength-sized plasmonic nanoantenna, are able to achieve phase modulation at full depth (from 0 to 2π), proving a versatile methodology for free-space light routing [99, 100, 103]. The polarization of the focused light after a conventional lens is mostly similar to that of the incident light. A metalens can be designed to realize novel focusing properties that a conventional lens cannot easily achieve. One example is focusing cross-polarized scattered light (i.e., the scattered polarization is perpendicular to the incident polarization) with a well-designed metalens [99] as shown in Figure 13b. The metalens consists of circular array of nano-voids that enable scattering the incident light with cross-polarized states and modulating the phase of the scattered light. Figures 13c and 13d show the intensity profiles of the cross-polarized scattered light at three perpendicular planes at the transmission side of the metalens. It can be seen that the cross-polarized scattered light is nicely focused about $9\ \mu\text{m}$ above the metalens when the illumination wavelength is 531 nm. Instead of converting linearly polarized light to the cross-polarized one, Chen et al. designed an ultrathin flat lens with focusing properties that depend on the helicity of circularly polarized light [100]. The full range of phase modulation from 0 to 2π is achieved by adjusting the orientation angle of the individual dipole antenna in an array as shown in the inset of Figure 13e. Figures 13e and 13f demonstrate that the flat lens behaves either as a converging or diverging lens, depending on the polarization state of the incident light with either right or left circular polarization, respectively. Other types of plasmonic lenses based on encoded metallic nanostructures with unique properties, such as aberration-free [103] and broadband focusing [104], have been developed as well. These metalenses with nanoantennas as building blocks significantly increase the design freedoms and thus pave a new way for designing compact flat lenses with functionalities unobtainable in conventional ones.

Light can carry two components of angular momentum; one is orbital angular momentum that depends on the field spatial distribution and the other is spin angular momentum

related to the light polarization. The spin-orbital interaction can happen as light propagates, and the manifestation of this coupling is the so-called optical spin Hall effect (OSHE). The OSHE is extremely weak and hard to detect without using sensitive detect techniques [108] or well designed structures [109] because of the inherently small photon spin-orbit interaction. Encoded plasmonic nanostructures have been successfully employed for detecting the OSHE recently. A strong spin-orbit interaction of light was experimentally demonstrated on a thin metasurface consists of V-shaped gold nanoantennas. Interestingly, large transverse motion of the circularly polarized light can be observed even at normal incidence, which does not exist on the interface between two homogeneous media, thanks to the rapidly varying phase discontinuities along the metasurface that result in the axial symmetry breaking [110]. The OSHE has also been demonstrated with a plasmonic slit [111] and concentric Z shaped apertures [112]. Hasman's group has conducted intensive investigations of the spin-orbit interaction of light with various metasurfaces [105, 113–117]. The OSHE can be realized by either designing the path curvature of local unit cell or the orientation of the local unit cell's anisotropy, which expands the scope of the OSHE and paves the way for engineering optical vortex beams with angular momentums. Figures 14a and 14b show the far-field diffraction pattern of the spin-flip component (the opposite spin state undergoes diffraction with respect to that of the incident light) with topological charge $l = 2$ and 4 from two circular plasmonic chains, which comprise circular and rotating rectangular apertures, respectively. Notice the dark spot in the center is a characteristic of optical vortex beams with orbital angular momentums. The radius of the dark spot generated from the rectangular chains is larger than that generated from the circular chains, corresponding to a higher orbital angular momentum. Recently, Sun et al. generated optical vortex beams using an array of nano waveguides that consists of PMMA filled nanoholes on a thick silver film [106]. The spiral pattern shown in Figure 14c is a result of the interference of a Gaussian beam and the generated vortex beam. The singularity revealed in the beam pattern is a characteristic of the optical vortex beam. Optical vortex can also be generated with closed-path nanoslit [118]. Lin et al. show that it is possible to convert circular polarization to radial polarization with a metasurface that is a superposition of a radial polarizer and a fork diffraction hologram as shown in the inset of Figure 14d [107]. Figure 14d presents the final light pattern with a radial polarization after illuminating the structure with a right circularly polarized light. Alù's group successfully demonstrated ultrathin quarter-wave plates based on plasmonic metasurfaces that enable manipulating the light polarizations [119].

Very recently, encoded nanostructures have also been successfully employed in optical holography. As a 3D image restructuring technique, conventional holography is either recorded in photo-sensitive materials (such as photoresists or photorefractives) by interference of the scattered beam from a real object with a reference beam, or fabricated with computer generated pixilated structures made of subwavelength grating [120] or multilayer metamaterial [121]. However, the complete phase control over the holography relies on the difference of the refractive index changes that result in the size of the pixilated structures in the range of wavelength-scale or

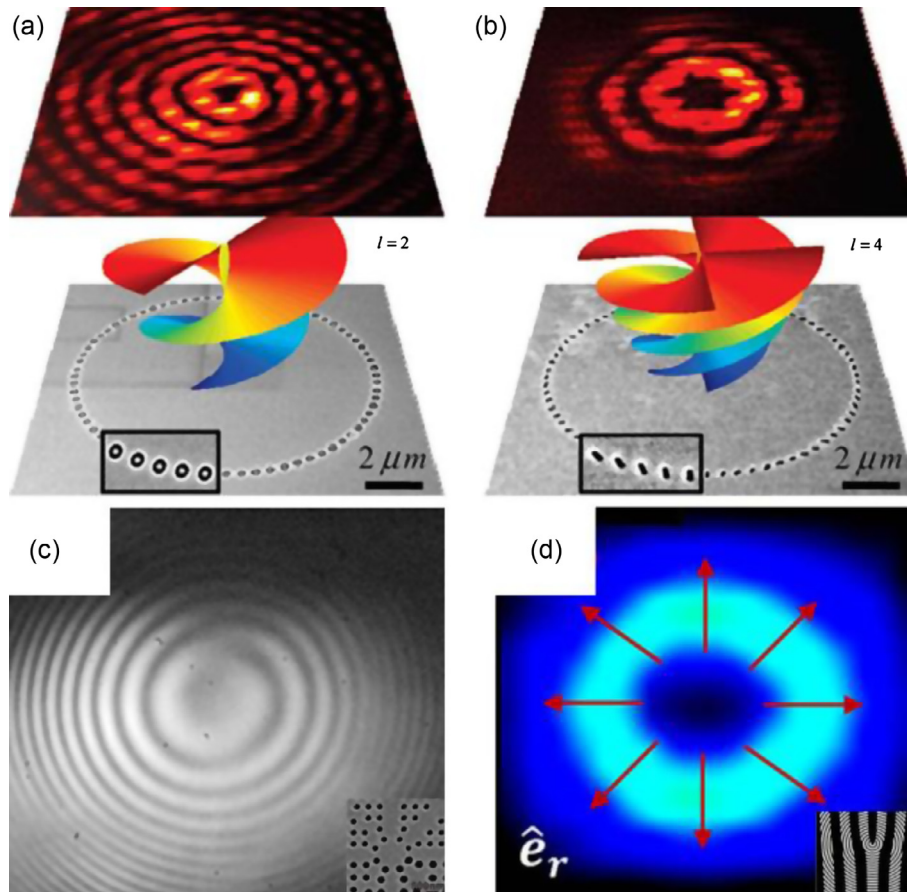


Figure 14. The measured far-field intensity distribution of the spin-flip component from a circular chain of ordered nanostructures (a) and rotating nanorods (b). Reprinted from reference [105] with permission. (c) Measured far-field optical vortex beams generated with array of nano waveguides filled with PMMA. Inset shows the SEM image of the structure. Reprinted from reference [106] with permission. (d) Generation of light with radial polarization with a metasurface. Inset show the schematic of the structure. Reprinted from reference [107] with permission.

even larger. In contrast, ultra-small and ultra-thin holograms can be implemented with metallic nanostructures as the pixels in the plasmonic holography by utilizing the full-phase modulation of these metallic nanostructures. Huang et al. demonstrated an ultrathin plasmonic holography consists of an array of plasmonic dipole antennas [122]. Encoding phase information in the holography is realized by changing the orientation of each dipole antenna. Such an innovative approach greatly simplifies the designing process. The phase change that occurs on the dipole antennas for circularly polarized light when converted to its opposite helicity ranges from 0 to 2π , enabling to fully recover the phase information. Figure 15a shows the reconstructed image of a solid jet from the plasmonic holography. There is a real and virtual image located at both sides of the holography. Almost at the same time, Ni et al. independently demonstrated an ultrathin plasmonic holography made of nano-voids of different shapes fabricated on a thin gold film [123]. A linearly polarized light at visible wavelengths is used to illuminate the holography and the reconstructed image is recoded at the cross polarized state. Figure 15b shows that a letter “PURDUE” is successfully

recovered 10 μm away from the surface of the plasmonic holography.

6 Perspectives

We have seen rapid development in the field of light manipulation with 2D encoded nanostructures in recent years. The encoded 2D nanostructures with its shape and position precisely controllable on a single interface provide numerous possibilities for diverse applications. Unlike the conventional refractive or DOE that modulate light based on phase accumulation via curvature or thickness variation of a bulk material, the encoded 2D metallic nanosurfaces, on the other hand, modulate light based on plasmonic-resonance related phase variation. This new scheme results in reduced device thickness and significantly simplifies the fabrication process. Tremendous progresses have been achieved in this field with various functional plasmonic devices being demonstrated. Novel concepts and designs continue emerging to push this field forward. Here, we provide perspectives as follows for the future

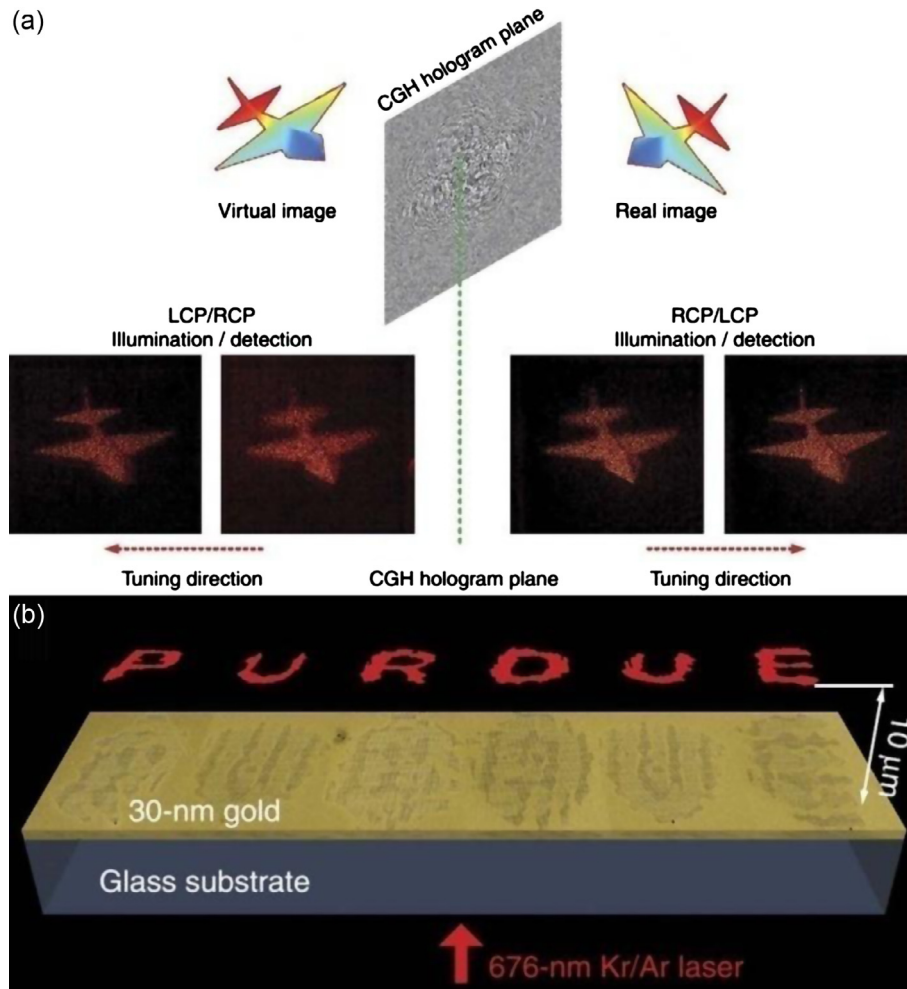


Figure 15. Plasmonic holography. (a) Demonstration of the real and the virtual images of a jet with plasmonic holography. Reprinted from reference [122] with permission. (b) Holographic image of a word “PURDUE” produced by metasurface holograms. Reprinted from reference [123] with permission.

development in this area:

1. *Multifunction and integration:* Although various functional plasmonic structures have been developed, their functionalities are typically limited. There are great demands for developing single plasmonic structures with multiple functionalities and compatibly integrating individual single-function plasmonic structures together to form complex functionalities. For example, Brongersma’s group recently demonstrated an electrically driven plasmonic nanocircuit that combines functions such as SPP routing, splitting, free-space coupling and directional coupling on one chip [124]. Kriesch et al. reported plasmonic nanocircuits with low insertion and propagation losses [125]. Atwater’s group recently demonstrated a resonant plasmonic network with V-groove channel plasmon polariton (CPP) waveguides as building block [126]. The results clearly manifest the promise of plasmonic integration in the real world, and more efforts should be devoted along this direction.
2. *Plasmonic loss compensation:* Although plasmonic nanocircuits that integrate individual functional plasmonic structures result in smaller footprint, compared to the silicon photonic circuits, one obstacle that hinders further massive integration is the propagation losses caused by metal absorption. Therefore, compensating the losses becomes the first priority in designing plasmonic devices. Fortunately, tremendous research efforts have been stimulated in exploring the feasibility of achieving SPP loss compensation and even lasing [40, 42, 43, 94, 127–131]. Most of these work used optical pumping. The electrical pumping technique, which is more preferential in integrated plasmonic circuits, is yet to be developed to compensate the plasmonic losses of the aforementioned encoded metallic nanostructures.
3. *Nanoscale heat engineering:* We can take advantage of the heat generation associated with plasmonic losses in some respects. For example, there is growing interest in controlling the temperatures at nanoscale with plasmonic nanostructures, so-called thermal plasmonics [132–137]. Under light illumination at plasmonic

resonance, the enhanced absorption of plasmonic nanostructure turns into an ideal remotely controllable nanoscale heating source. The encoded metallic nanostructures provide a flexible way of converting the SPP energy and the associated heating into a specified area on a metal film. In addition, we may use metasurface to control the direction of blackbody radiation [138, 139].

4. *Integration with silicon photonic elements*: Another promising direction is integrating plasmonic devices with silicon photonics. Silicon photonic devices that share the commercial complementary metal-oxide semiconductor (CMOS) chip fabrication facilities have witnessed fast development in recent years [140–143] and will be very likely commercialized in the near future. The silicon photonic devices do not suffer much from absorption losses; however, it is limited by their sizes due to the diffraction limit. Plasmonic functional elements with sub-wavelength scales, on the other hand, can fit on a silicon photonic chip where ultra-small, ultra-fast plasmonic functional elements are prerequisite. For example, a new ultra-compact high-speed plasmonic phase modulator integrated with Si waveguides has been demonstrated very recently [144]. The device operates at speed as high as 40 Gbit s^{-1} , manifesting great potential for integration with next generation high-speed photonic platforms. The efficient coupling between plasmonic and silicon elements is critical. Atwater's group reported low insertion loss for dielectric-loaded plasmonic waveguides end-coupled to silicon waveguides with a coupling efficiency as high as 80% at telecommunication wavelengths [145].
5. *Approaching the quantum region*: Last but not least, the quantum aspect of plasmonic, or quantum plasmonics [146, 147], is an extremely exciting topic to pursue. This field has shown rapid growth over the past years. The wave-particle duality, a fundamental property of quantum mechanics, has been proven valid for single SPPs as well [148]. Lukin's group has generated single SPPs in a metallic nanowire coupled with a quantum dot [149]. Very recently, Atwater's group demonstrated two-plasmon quantum interference [150]. The quantum property of the incident light from the free space survives through the conversion between photons and surface plasmons. The versatile SPP manipulation method based on the encoded plasmonic nanostructures is also ideal for performing quantum simulations, where one quantum system is simulated by using another more accessible physical system [151, 152]. The 2D nature of the SPP field together with the easy accessible 2D field mapping by using leakage radiation microscopy [31, 32] makes the design and visualization of the quantum simulation much easier. Block et al. recently demonstrated Bloch oscillations in a plasmonic system that consists of plasmonic waveguide arrays. This oscillation is a plasmonic analogue of the Bloch oscillation of an electronic wave packet in a crystal when a static external field is applied. The linear potential associated with the

static external field applied to a crystal was mimicked by a linear increased effective refractive index of the plasmonic waveguide [153]. These findings provide great promise for developing quantum plasmonic devices based on the encoded metallic structures.

References

1. S.I. Bozhevolnyi, V.S. Volkov, E. Devaux, J.-Y. Laluet, T.W. Ebbesen, *Nature* 440 (2006) 508.
2. H.A. Atwater, A. Polman, *Nat. Mater.* 9 (2010) 205.
3. S. Linic, P. Christopher, D.B. Ingram, *Nat. Mater.* 10 (2011) 911.
4. W. Cai, V. Shalaev, *Optical metamaterials: fundamentals and applications*, Springer, New York, 2010.
5. Y. Liu, X. Zhang, *Chem. Soc. Rev.* 40 (2011) 2494.
6. C.M. Soukoulis, M. Wegener, *Nat. Photonics* 5 (2011) 523.
7. K. Yao, Y. Liu, *Nanotechnol. Rev.* 3 (2014) 117.
8. X. Zhang, Z. Liu, *Nat. Mater.* 7 (2008) 435.
9. J.B. Pendry, *Phys. Rev. Lett.* 85 (2000) 3966.
10. N. Fang, H. Lee, C. Sun, X. Zhang, *Science* 308 (2005) 534.
11. S.C. Kehr, Y.M. Liu, L.W. Martin, P. Yu, M. Gajek, S.-Y. Yang, C.-H. Yang, M.T. Wenzel, R. Jacob, H.-G. von Ribbeck, M. Helm, X. Zhang, L.M. Eng, R. Ramesh, *Nat. Commun.* 2 (2011) 249.
12. M.A. Schmidt, D.Y. Lei, L. Wondraczek, V. Nazabal, S.A. Maier, *Nat. Commun.* 3 (2012) 1108.
13. A.V. Kabashin, P. Evans, S. Pastkovsky, W. Hendren, G.A. Wurtz, R. Atkinson, R. Pollard, V.A. Podolskiy, A.V. Zayats, *Nat. Mater.* 8 (2009) 867.
14. K.A. Willets, R.P. Van Duyne, *Annu. Rev. Phys. Chem.* 58 (2007) 267.
15. J.N. Anker, W.P. Hall, O. Lyandres, N.C. Shah, J. Zhao, R.P. Van Duyne, *Nat. Mater.* 7 (2008) 442.
16. N. Yu, F. Capasso, *Nat. Mater.* 13 (2014) 139.
17. N. Yu, P. Genevet, M.A. Kats, F. Aieta, J.-P. Tetienne, F. Capasso, Z. Gaburro, *Science* 334 (2011) 333.
18. A. Archambault, T.V. Teperik, F. Marquier, J.J. Greffet, *Phys. Rev. B* 79 (2009) 195414.
19. S.A. Maier, *Plasmonics: fundamentals and applications*, Springer, New York, 2007.
20. E.T. Arakawa, M.W. Williams, R.N. Hamm, R.H. Ritchie, *Phys. Rev. Lett.* 31 (1973) 1127.
21. R.W. Alexander, G.S. Kovener, R.J. Bell, *Phys. Rev. Lett.* 32 (1974) 154.
22. A. Polman, *Science* 322 (2008) 868.
23. S.-H. Chang, S.K. Gray, G.C. Schatz, *Opt. Express* 13 (2005) 3150.
24. J. Wang, X. Wu, J. Zhang, *Opt. Express* 18 (2010) 6686.
25. A. Archambault, T. Teperik, F. Marquier, J. Greffet, *Phys. Rev. B* 79 (2009) 195414.
26. C. Zhao, J. Zhang, *Appl. Phys. Lett.* 98 (2011) 211108.
27. C. Zhao, J. Wang, X. Wu, J. Zhang, *Appl. Phys. Lett.* 94 (2009) 111105.
28. C. Zhao, J. Zhang, *Opt. Lett.* 34 (2009) 2417.
29. C. Zhao, J. Zhang, *ACS Nano* 4 (2010) 6433.

30. W. Zhang, C. Zhao, J. Wang, J. Zhang, *Opt. Express* 17 (2009) 19757.
31. B. Hecht, H. Bielefeldt, L. Novotny, Y. Inouye, D. Pohl, *Phys. Rev. Lett.* 77 (1996) 1889.
32. A. Drezet, A. Hohenau, A.L. Stepanov, H. Ditlbacher, B. Steinberger, N. Galler, F.R. Aussenegg, A. Leitner, J.R. Krenn, *Appl. Phys. Lett.* 89 (2006) 091117.
33. J. Wang, C. Zhao, J. Zhang, *Opt. Lett.* 35 (2010) 1944.
34. A. Hohenau, J.R. Krenn, A. Drezet, O. Mollet, S. Huant, C. Genet, B. Stein, T.W. Ebbesen, *Opt. Express* 19 (2011) 25749.
35. A. Drezet, C. Genet, *Phys. Rev. Lett.* 110 (2013) 213901.
36. D.K. Gramotnev, S.I. Bozhevolnyi, *Nat. Photonics* 4 (2010) 83.
37. Z. Wang, H. Wei, D. Pan, H. Xu, *Laser Photon. Rev.* 8 (2014) 596.
38. M.A. Noginov, G. Zhu, A.M. Belgrave, R. Bakker, V.M. Shalaev, E.E. Narimanov, S. Stout, E. Herz, T. Suteewong, U. Wiesner, *Nature* 460 (2009) 1110.
39. R.-M. Ma, R.F. Oulton, V.J. Sorger, G. Bartal, X. Zhang, *Nat. Mater.* 10 (2011) 110.
40. I. De Leon, P. Berini, *Nat. Photonics* 4 (2010) 382.
41. R.F. Oulton, V.J. Sorger, T. Zentgraf, R.-M. Ma, C. Gladden, L. Dai, G. Bartal, X. Zhang, *Nature* 461 (2009) 629.
42. M.T. Hill, Y.-S. Oei, B. Smalbrugge, Y. Zhu, T. de Vries, P.J. van Veldhoven, F.W.M. van Otten, T.J. Eijkemans, J.P. Turkievicz, H. de Waardt, E.J. Geluk, S.-H. Kwon, Y.-H. Lee, R. Nötzel, M.K. Smit, *Nat. Photonics* 1 (2007) 589.
43. P. Berini, I. De Leon, *Nat. Photonics* 6 (2011) 16.
44. M.P. Nezhad, A. Simic, O. Bondarenko, B. Slutsky, A. Mizrahi, L. Feng, V. Lomakin, Y. Fainman, *Nat. Photonics* 4 (2010) 395.
45. D. Bergman, M. Stockman, *Phys. Rev. Lett.* 90 (2003) 027402.
46. N. Rotenberg, M. Betz, H.M. van Driel, *Phys. Rev. Lett.* 105 (2010) 17402.
47. F. López-Tejiera, S.G. Rodrigo, L. Martín-Moreno, F.J. García-Vidal, E. Devaux, T.W. Ebbesen, J.R. Krenn, I.P. Radko, S.I. Bozhevolnyi, M.U. González, J.C. Weeber, A. Dereux, *Nat. Phys.* 3 (2007) 324.
48. J. Chen, Z. Li, X. Zhang, J. Xiao, Q. Gong, *Sci. Rep.* 3 (2013) 1451.
49. F.J. Rodríguez-Fortuño, G. Marino, P. Ginzburg, D. O'Connor, A. Martínez, G.A. Wurtz, A.V. Zayats, *Science* 340 (2013) 328.
50. F. López-Tejiera, S.G. Rodrigo, L. Martín-Moreno, F.J. García-Vidal, E. Devaux, J. Dintinger, T.W. Ebbesen, J.R. Krenn, I.P. Radko, S.I. Bozhevolnyi, M.U. González, J.C. Weeber, A. Dereux, *New J. Phys.* 10 (2008) 033035.
51. H. Liao, Z. Li, J. Chen, X. Zhang, S. Yue, Q. Gong, *Sci. Rep.* 3 (2013) 1918.
52. X. Li, Q. Tan, B. Bai, G. Jin, *Appl. Phys. Lett.* 98 (2011) 251109.
53. H. Kim, B. Lee, *Plasmonics* 4 (2009) 153.
54. S.-Y. Lee, I.-M. Lee, J. Park, S. Oh, W. Lee, K.-Y. Kim, B. Lee, *Phys. Rev. Lett.* 108 (2012) 213907.
55. X. Huang, M.L. Brongersma, *Nano Lett.* 13 (2013) 5420.
56. A. Baron, E. Devaux, J.-C. Rodier, J.-P. Hugonin, E. Rousseau, C. Genet, T.W. Ebbesen, P. Lalanne, *Nano Lett.* 11 (2011) 4207.
57. N. Bonod, E. Popov, L. Li, B. Chernov, *Opt. Express* 15 (2007) 11427.
58. I.P. Radko, S.I. Bozhevolnyi, G. Brucoli, L. Martín-Moreno, F.J. García-Vidal, A. Boltasseva, *Opt. Express* 17 (2009) 7228.
59. Y. Liu, S. Palomba, Y. Park, T. Zentgraf, X. Yin, X. Zhang, *Nano Lett.* 12 (2012) 4853.
60. J. Yang, X. Xiao, C. Hu, W. Zhang, S. Zhou, J. Zhang, *Nano Lett.* 14 (2014) 704.
61. V. Giannini, A.I. Fernández-Domínguez, S.C. Heck, S.A. Maier, *Chem. Rev.* 111 (2011) 3888.
62. P. Mühlischlegel, H.-J. Eisler, O.J.F. Martin, B. Hecht, D.W. Pohl, *Science* 308 (2005) 1607.
63. L. Novotny, N. Van Hulst, *Nat. Photonics* 5 (2011) 83.
64. J. Yang, S. Zhou, C. Hu, W. Zhang, X. Xiao, J. Zhang, *Laser Photon. Rev.* 8 (2014) 590.
65. J. Lin, J.P.B. Mueller, Q. Wang, G. Yuan, N. Antoniou, X.-C. Yuan, F. Capasso, *Science* 340 (2013) 331.
66. L. Huang, X. Chen, B. Bai, Q. Tan, G. Jin, T. Zentgraf, S. Zhang, *Light Sci. Appl.* 2 (2013) e70.
67. B. Stein, J.-Y. Laluet, E. Devaux, C. Genet, T.W. Ebbesen, *Phys. Rev. Lett.* 105 (2010) 266804.
68. B. Stein, E. Devaux, C. Genet, T.W. Ebbesen, *Opt. Lett.* 37 (2012) 1916.
69. T. Zentgraf, Y. Liu, M.H. Mikkelsen, J. Valentine, X. Zhang, *Nat. Nanotechnol.* 6 (2011) 151.
70. G.M. Lerman, U. Levy, *Nano Lett.* 13 (2013) 1100.
71. G.M. Lerman, A. Yanai, U. Levy, *Nano Lett.* 9 (2009) 2139.
72. Z. Liu, J.M. Steele, W. Srituravanich, Y. Pikus, C. Sun, X. Zhang, *Nano Lett.* 5 (2005) 1726.
73. W. Chen, D.C. Abeysinghe, R.L. Nelson, Q. Zhan, *Nano Lett.* 9 (2009) 4320.
74. H. Kim, J. Park, S.-W. Cho, S.-Y. Lee, M. Kang, B. Lee, *Nano Lett.* 10 (2010) 529.
75. H.L. Offerhaus, B. van den Bergen, M. Escalante, F.B. Segerink, J.P. Korterik, N.F. van Hulst, *Nano Lett.* 5 (2005) 2144.
76. L. Yin, V.K. Vlasko-Vlasov, J. Pearson, J.M. Hiller, J. Hua, U. Welp, D.E. Brown, C.W. Kimball, *Nano Lett.* 5 (2005) 1399.
77. S. Cherukulappurath, D. Heinis, J. Cesario, N.F. van Hulst, S. Enoch, R. Quidant, *Opt. Express* 17 (2009) 23772.
78. Y. Hua, J.Y. Suh, W. Zhou, M.D. Huntington, T.W. Odom, *Opt. Express* 20 (2012) 14284.
79. D. van Oosten, M. Spasenović, L. Kuipers, *Nano Lett.* 10 (2010) 286.
80. J. Wang, C. Hu, J. Zhang, *Opt. Express* 22 (2014) 22753.
81. L. Li, T. Li, S. Wang, S. Zhu, X. Zhang, *Nano Lett.* 11 (2011) 4357.
82. T. Tanemura, K.C. Balram, D.-S. Ly-Gagnon, P. Wahl, J.S. White, M.L. Brongersma, D.A.B. Miller, *Nano Lett.* 11 (2011) 2693.
83. J.S.Q. Liu, R.A. Pala, F. Afshinmanesh, W. Cai, M.L. Brongersma, *Nat. Commun.* 2 (2011) 525.
84. S. Zhang, Z. Ye, Y. Wang, Y. Park, G. Bartal, M. Mrejen, X. Yin, X. Zhang, *Phys. Rev. Lett.* 109 (2012) 193902.
85. A. Minovich, A.E. Klein, N. Janunts, T. Pertsch, D.N. Neshev, Y.S. Kivshar, *Phys. Rev. Lett.* 107 (2011) 116802.
86. J. Lin, J. Dellinger, P. Genevet, B. Cluzel, F. de Fornel, F. Capasso, *Phys. Rev. Lett.* 109 (2012) 093904.
87. L. Li, T. Li, S.M. Wang, C. Zhang, S.N. Zhu, *Phys. Rev. Lett.* 107 (2011) 126804.
88. P. Zhang, S. Wang, Y. Liu, X. Yin, C. Lu, Z. Chen, X. Zhang, *Opt. Lett.* 36 (2011) 3191.
89. A. Salandrino, D.N. Christodoulides, *Opt. Lett.* 35 (2010) 2082.
90. A.E. Minovich, A.E. Klein, D.N. Neshev, T. Pertsch, Y.S. Kivshar, D.N. Christodoulides, *Laser Photon. Rev.* 8 (2014) 221.

91. L. Li, T. Li, S. Wang, S. Zhu, *Phys. Rev. Lett.* 110 (2013) 046807.
92. I. Dolev, I. Epstein, A. Arie, *Phys. Rev. Lett.* 109 (2012) 203903.
93. C. Zhao, Y. Liu, Y. Zhao, N. Fang, T.J. Huang, *Nat. Commun.* 4 (2013) 2305.
94. K.F. MacDonald, N.I. Zheludev, *Laser Photon. Rev.* 4 (2009) 562.
95. V.V. Temnov, G. Armelles, U. Woggon, D. Guzatov, A. Cebollada, A. Garcia-Martin, J.-M. Garcia-Martin, T. Thomay, A. Leitenstorfer, R. Bratschitsch, *Nat. Photonics* 4 (2010) 107.
96. B. Gjonaj, J. Aulbach, P.M. Johnson, A.P. Mosk, L. Kuipers, A. Lagendijk, *Nat. Photonics* 5 (2011) 360.
97. N. Mohammadi Estakhri, A. Alù, *Phys. Rev. B* 89 (2014) 235419.
98. H. Gao, J.K. Hyun, M.H. Lee, J.-C. Yang, L.J. Lauhon, T.W. Odom, *Nano Lett.* 10 (2010) 4111.
99. X. Ni, S. Ishii, A.V. Kildishev, V.M. Shalaev, *Light Sci. Appl.* 2 (2013) e72.
100. X. Chen, L. Huang, H. Mühlenbernd, G. Li, B. Bai, Q. Tan, G. Jin, C.-W. Qiu, S. Zhang, T. Zentgraf, *Nat. Commun.* 3 (2012) 1198.
101. L. Verslegers, P.B. Catrysse, Z. Yu, J.S. White, E.S. Barnard, M.L. Brongersma, S. Fan, *Nano Lett.* 9 (2009) 235.
102. L. Lin, X.M. Goh, L.P. McGuinness, A. Roberts, *Nano Lett.* 10 (2010) 1936.
103. F. Aieta, P. Genevet, M.A. Kats, N. Yu, R. Blanchard, Z. Gaburro, F. Capasso, *Nano Lett.* 12 (2012) 4932.
104. A. Pors, M.G. Nielsen, R.L. Eriksen, S.I. Bozhevolnyi, *Nano Lett.* 13 (2013) 829.
105. N. Shitrit, I. Bretner, Y. Gorodetski, V. Kleiner, E. Hasman, *Nano Lett.* 11 (2011) 2038.
106. J. Sun, X. Wang, T. Xu, Z. Kudyshev, A.N. Cartwright, N.M. Litchinitser, *Nano Lett.* 14 (2014) 2726.
107. J. Lin, P. Genevet, M.A. Kats, N. Antoniou, F. Capasso, *Nano Lett.* 13 (2013) 4269.
108. O. Hosten, P. Kwiat, *Science* 319 (2008) 787.
109. K.Y. Bliokh, A. Niv, V. Kleiner, E. Hasman, *Nat. Photonics* 2 (2008) 748.
110. X. Yin, Z. Ye, J. Rho, Y. Wang, X. Zhang, *Science* 339 (2013) 1405.
111. Y. Gorodetski, K.Y. Bliokh, B. Stein, C. Genet, N. Shitrit, V. Kleiner, E. Hasman, T.W. Ebbesen, *Phys. Rev. Lett.* 109 (2012) 013901.
112. G. Li, M. Kang, S. Chen, S. Zhang, E.Y.-B. Pun, K.W. Cheah, J. Li, *Nano Lett.* 13 (2013) 4148.
113. N. Shitrit, S. Nechayev, V. Kleiner, E. Hasman, *Nano Lett.* 12 (2012) 1620.
114. N. Shitrit, I. Yulevich, E. Maguid, D. Ozeri, D. Veksler, V. Kleiner, E. Hasman, *Science* 340 (2013) 724.
115. Y. Gorodetski, N. Shitrit, I. Bretner, V. Kleiner, E. Hasman, *Nano Lett.* 9 (2009) 3016.
116. Y. Gorodetski, A. Niv, V. Kleiner, E. Hasman, *Phys. Rev. Lett.* 101 (2008) 043903.
117. Y. Gorodetski, S. Nechayev, V. Kleiner, E. Hasman, *Phys. Rev. B* 82 (2010) 125433.
118. E. Brasselet, G. Gervinskas, G. Seniutinas, S. Juodkazis, *Phys. Rev. Lett.* 111 (2013) 193901.
119. Y. Zhao, A. Alù, *Phys. Rev. B* 84 (2011) 205428.
120. U. Levy, H.-C. Kim, C.-H. Tsai, Y. Fainman, *Opt. Lett.* 30 (2005) 2089.
121. S. Larouche, Y.-J. Tsai, T. Tyler, N.M. Jokerst, D.R. Smith, *Nat. Mater.* 11 (2012) 450.
122. L. Huang, X. Chen, H. Mühlenbernd, H. Zhang, S. Chen, B. Bai, Q. Tan, G. Jin, K.-W. Cheah, C.-W. Qiu, J. Li, T. Zentgraf, S. Zhang, *Nat. Commun.* 4 (2013) 2808.
123. X. Ni, A.V. Kildishev, V.M. Shalaev, *Nat. Commun.* 4 (2013) 2807.
124. K.C.Y. Huang, M.-K. Seo, T. Sarmiento, Y. Huo, J.S. Harris, M.L. Brongersma, *Nat. Photonics* 8 (2014) 244.
125. A. Kriesch, S.P. Burgos, D. Ploss, H. Pfeifer, H.A. Atwater, U. Peschel, *Nano Lett.* 13 (2013) 4539.
126. S.P. Burgos, H.W. Lee, E. Feigenbaum, R.M. Briggs, H.A. Atwater, *Nano Lett.* 14 (2014) 3284.
127. D.Y. Fedyanin, A.V. Krasavin, A.V. Arsenin, A.V. Zayats, *Nano Lett.* 12 (2012) 2459.
128. A.V. Krasavin, T.P. Vo, W. Dickson, P.M. Bolger, A.V. Zayats, *Nano Lett.* 11 (2011) 2231.
129. A.V. Krasavin, N.I. Zheludev, *Appl. Phys. Lett.* 84 (2004) 1416.
130. J. Grandidier, G.C. des Francs, S. Massenot, A. Bouhelier, L. Markey, J.-C. Weeber, C. Finot, A. Dereux, *Nano Lett.* 9 (2009) 2935.
131. P.M. Bolger, W. Dickson, A.V. Krasavin, L. Liebscher, S.G. Hickey, D.V. Skryabin, A.V. Zayats, *Opt. Lett.* 35 (2010) 1197.
132. G. Baffou, C. Girard, R. Quidant, *Phys. Rev. Lett.* 104 (2010) 136805.
133. G. Baffou, R. Quidant, F.J. García de Abajo, *ACS Nano* 4 (2010) 709.
134. J.B. Herzog, M.W. Knight, D. Natelson, *Nano Lett.* 14 (2014) 499.
135. G. Baffou, P. Berto, E. Bermúdez Ureña, R. Quidant, S. Monneret, J. Polleux, H. Rigneault, *ACS Nano* 7 (2013) 6478.
136. A. Sanchot, G. Baffou, R. Marty, A. Arbouet, R. Quidant, C. Girard, E. Dujardin, *ACS Nano* 6 (2012) 3434.
137. G. Baffou, R. Quidant, *Laser Photon. Rev.* 7 (2013) 171.
138. A. Babuty, K. Joulain, P.-O. Chapuis, J.-J. Greffet, Y. De Wilde, *Phys. Rev. Lett.* 110 (2013) 146103.
139. T.V. Shahbazyan, M.I. Stockman (Eds.), *Plasmonics: theory and applications*, Springer Netherlands, Dordrecht, 2013.
140. N.C. Harris, Y. Ma, J. Mower, T. Baehr-Jones, D. Englund, M. Hochberg, C. Galland, *Opt. Express* 22 (2014) 10487.
141. J.S. Levy, A. Gondarenko, M.A. Foster, A.C. Turner-Foster, A.L. Gaeta, M. Lipson, *Nat. Photonics* 4 (2009) 37.
142. L. Razzari, D. Duchesne, M. Ferrera, R. Morandotti, S. Chu, B.E. Little, D.J. Moss, *Nat. Photonics* 4 (2009) 41.
143. H. Guan, A. Novack, M. Streshinsky, R. Shi, Q. Fang, A.E.-J. Lim, G.-Q. Lo, T. Baehr-Jones, M. Hochberg, *Opt. Express* 22 (2014) 2489.
144. A. Melikyan, L. Alloatti, A. Muslija, D. Hillerkuss, P.C. Schindler, J. Li, R. Palmer, D. Korn, S. Muehlbrandt, D. Van Thourhout, B. Chen, R. Dinu, M. Sommer, C. Koos, M. Kohl, W. Freude, J. Leuthold, *Nat. Photonics* 8 (2014) 229.
145. R.M. Briggs, J. Grandidier, S.P. Burgos, E. Feigenbaum, H.A. Atwater, *Nano Lett.* 10 (2010) 4851.
146. Z. Jacob, *MRS Bull.* 37 (2012) 761.
147. M.S. Tame, K.R. McEnery, Ş.K. Özdemir, J. Lee, S.A. Maier, M.S. Kim, *Nat. Phys.* 9 (2013) 329.

148. R. Kolesov, B. Grotz, G. Balasubramanian, R.J. Stöhr, A.A.L. Nicolet, P.R. Hemmer, F. Jelezko, J. Wrachtrup, *Nat. Phys.* 5 (2009) 470.
149. A.V. Akimov, A. Mukherjee, C.L. Yu, D.E. Chang, A.S. Zibrov, P.R. Hemmer, H. Park, M.D. Lukin, *Nature* 450 (2007) 402.
150. J.S. Fakonas, H. Lee, Y.A. Kelaita, H.A. Atwater, *Nat. Photonics* 8 (2014) 317.
151. T. Schaetz, C.R. Monroe, T. Esslinger, *New J. Phys.* 15 (2013) 085009.
152. A. Aspuru-Guzik, P. Walther, *Nat. Phys.* 8 (2012) 285.
153. A. Block, C. Etrich, T. Limboeck, F. Bleckmann, E. Soergel, C. Rockstuhl, S. Linden, *Nat. Commun.* 5 (2014) 3843.

Cite this article as: Zhao C, Zhang J & Liu Y: Light manipulation with encoded plasmonic nanostructures. *EPJ Appl. Metamat.* 2014, 1, 6.